NASA TN D-245

TECHNICAL NOTE
D-245

COMPRESSIBILITY EFFECTS ON THE HOVERING PERFORMANCE OF A TWO-BLADE 10-FOOT-DIAMETER HELICOPTER ROTOR OPERATING AT TIP MACH NUMBERS UP TO 0.98

By Joseph W. Jewel, Jr.

Langley Research Center
Langley Field, Va.

NATIONAL AERONAUTICS AND SPACE ADMINISTRATION

WASHINGTON April 1960

NATIONAL AERONAUTICS AND SPACE ADMINISTRATION

TECHNICAL NOTE D-245

COMPRESSIBILITY EFFECTS ON THE HOVERING PERFORMANCE OF A TWO-BLADE 10-FOOT-DIAMETER HELICOPTER ROTOR OPERATING AT TIP MACH NUMBERS UP TO 0.98

By Joseph W. Jewel, Jr.

SUMMARY

Hovering tests have been conducted in the Langley full-scale tunnel on an all-metal two-blade helicopter rotor 10 feet in diameter. The rotor blades had an NACA 0012 airfoil section, a 2/1 taper ratio, -12° of twist, and a solidity of about 0.10. Performance curves are presented for tip Mach numbers from 0.09 to 0.98 and disk loadings as high as 22 pounds per square foot. Induced velocities 15 percent and 45 percent of the radius beneath the plane of the rotor are given for the maximum disk loads for a representative range of tip Mach numbers. Sound-pressure levels measured at a point about 30 feet from the center of rotation and on a radial line inclined 5° below the plane of rotation are included for all Mach numbers above 0.45 covered in the tests.

As the rotor tip speed was increased, compressibility losses occurred at progressively lower rotor mean lift coefficients. At tip Mach numbers of 0.90 and above, compressibility losses were present even at zero thrust. Induced velocity distribution beneath the plane of the rotor appeared to be relatively unaffected by tip Mach number. The major factor influencing the noise level of the rotor was tip speed. Smaller increases in noise were incurred by increases in thrust.

INTRODUCTION

As part of a continuing study of the effect of compressibility on performance characteristics of helicopter rotors, a rotor having two metal blades and a diameter of 10 feet has been tested in hovering to blade tip Mach numbers as high as 0.98. Blade geometry was generally similar to that of one set of the blades tested in reference 1 in that both sets had two blades, an NACA 0012 airfoil section, and a solidity of about 0.10; however, for these blades, a twist of -12° and a taper ratio of 2/1 were used.

The primary purpose of this test was to check the structural integrity of the blades; however, because data at tip Mach numbers near the speed of sound are quite meager, the measured rotor thrust and torque characteristics were obtained simultaneously with the structural tests and are the subject of this report. It is expected that the conditions in hovering for the start of the compressibility drag rise and its subsequent rate of change at different combinations of rotor-blade tip Mach numbers and mean blade loadings will provide some basis for rational design at other operating conditions. A limited number of measurements made in the rotor wake show the induced velocity distribution at 15 percent and 45 percent of the radius beneath the plane of the rotor. Some measurements of overall sound-pressure levels are also presented.

SYMBOLS

a slope of section-lift-coefficient curve as a function of section angle of attack, radians

B tip loss factor

b number of blades per rotor

C_Q rotor torque coefficient, $\frac{Q}{\pi R^2 \rho (\Omega R)^2 R}$

$C_{Q,o}$ rotor profile-drag torque coefficient, $\frac{Q_o}{\pi R^2 \rho (\Omega R)^2 R}$

C_T rotor thrust coefficient, $\frac{T}{\pi R^2 \rho (\Omega R)^2}$

c blade section chord, ft

c_e equivalent blade chord on thrust basis, $\frac{\int_0^R cr^2 dr}{\int_0^R r^2 dr}$, ft

$c_{d,o}$ section profile-drag coefficient

c_l section lift coefficient

$\bar{c}_l$	mean lift coefficient, $\frac{6C_T}{\sigma}$
I	mass moment of inertia of blade about flapping hinge, slug-ft^2
M	rotor figure of merit, $0.707\frac{C_T^{3/2}}{C_Q}$
M_t	blade tip Mach number (ratio of blade tip speed to speed of sound)
N_{Re}	Reynolds number, $\frac{\rho(\Omega r)c}{\mu}$
Q	rotor-shaft torque, lb-ft
Q_i	rotor induced-drag torque, lb-ft
Q_o	rotor profile-drag torque, lb-ft
R	blade radius, ft
r	radial distance to a blade element, ft
T	rotor thrust, lb
v	local induced velocity, ft/sec
v_o	rotor induced velocity, $\Omega R\sqrt{\frac{C_T}{2}}$
x	ratio of blade-element radius to rotor-blade radius, r/R
z	elevation above or below rotor (positive above rotor), ft
α_r	blade-element angle of attack, measured from line of zero lift, $\theta - \phi$, deg or radians
γ'	mass constant of rotor blade, $\frac{c_e\rho R^4}{I}$
θ	blade pitch angle, radians
μ	coefficient of viscosity for air, slugs/ft-sec

ρ mass density of air, slugs/cu ft

σ rotor solidity, $\frac{bc_e}{\pi R}$

σ_x local solidity of blade element at spanwise station x, $\frac{bc_x}{\pi R}$

ϕ inflow angle at blade element in plane perpendicular to blade-span axis, $\frac{\sigma_x a}{16x}\left(-1 + \sqrt{1 + \frac{32x\theta}{\sigma_x a}}\right)$, radians

Ω rotor angular velocity, radians/sec

Subscripts:

t rotor-blade tip

x at station x

APPARATUS AND TESTS

Rotor Blades

The rotor blades tested in this investigation were constructed from aluminum, magnesium, and fiber glass. The spar was aluminum and extended from the blade leading edge to about the 14-percent chord. Fiber-glass ribs, generally spaced 3 inches apart along the blade radius, were bonded to a fiber-glass and plastic U-channel which was, in turn, attached to the aluminum spar. The blade shell was then covered with a magnesium skin which was formed and bonded to the blade shell by means of a pressure mold. A photograph of the blade components before assembly is shown as figure 1. Plastic filler was used to form the blade leading edge to the desired airfoil contour. Rib compartments were vented near the trailing edge to relieve internal pressures created by centrifugal pumping action. Metal clips were fastened at intervals along the trailing edge to reinforce the juncture of the upper and lower surface skins. A photograph of a complete blade is shown as figure 2.

The rotor blades used had an NACA 0012 airfoil section, a 2/1 planform taper ratio, and -12° of twist. Templates indicated that the leading edges conformed to the true contour of the airfoil section and that the blades rearward of the spar were smooth and fair. The physical

characteristics of the blades are given in the following table:

Weight (blade alone), lb	14.14
Radius, ft	5.00
Chordwise center of gravity (blade alone), percent chord	25.00
Spanwise center of gravity (blade alone), percent span	43.80
c_e, in.	9.40
Tip chord, in.	7.60
Root chord (extrapolated to center-line rotation), in.	15.20
Twist, deg	-12.00
σ	0.099
γ' (blade alone)	0.44
I (blade alone), slug-ft^2	2.67
Airfoil section	NACA 0012

Blade-form curves are presented in figure 3.

For these tests, the rotor blades were mounted on a teetering or "see-saw" hub (fig. 4). The maximum flapping angles were restricted to $\pm 2^\circ$ to prevent interference between the blades and the wake-survey rakes which were mounted immediately below the plane of the rotor. The hub radius was 18 percent of the blade radius.

Rotor Support

The rotor hub was mounted on an extension shaft which was connected through a flexible coupling to the drive shaft of a 1,000-horsepower electric motor. The complete assembly was supported by the struts leading to the tunnel balance. The arrangement of the test apparatus in the Langley full-scale tunnel (described in ref. 2) is shown in figure 5.

Instrumentation

The following quantities were measured and recorded: rotor thrust, rotor torque, blade pitch, teetering angle, and rotor-shaft rotational speed. Rotor thrust was measured on the wind-tunnel balance and torque measurements were obtained from a strain-gage beam on the rotor shaft that measured the torque reaction of the drive motor. Blade pitch was manually set prior to each test, and a strain-gage beam monitored the pitch angle at the blade root throughout the test. Teetering angles were obtained from a strain-gage beam mounted at the hub teetering axis. An electromagnetic pickup was mounted on the rotor drive shaft to obtain rotational speed. The data measured on the rotating components were

transmitted through a 24-ring slipring assembly mounted on the bottom of the motor shaft.

Corrections for down loads from rotor downwash on the supporting structure were determined by calibrations of a scaled model and applied to the thrust measurements. This correction amounted to about 4 percent of the measured thrust. Torque tares were measured with the blades removed and were found to be insignificant. The estimated accuracies are as follows: thrust, ±5 pounds; torque, ±1/2 percent at 1,000 pound-feet; rotor speed, ±1/2 percent at 2,100 revolutions per minute; and angular measurements, ±0.05°.

Tests

The helicopter rotor used in the investigation was tested over a range of tip Mach numbers from 0.09 to 0.98. Tests at $M_t = 0.09$ were extended through blade stall. Maximum rotor mean lift coefficients varied from 0.88 at $M_t = 0.09$ to 0.39 at $M_t = 0.98$. The tests also included some measurements of the wake-velocity distribution and the sound-pressure level. Wake velocities were obtained by survey rakes having 20 total-pressure and 20 static-pressure tubes spaced along 118 percent of the blade radius and located 0.145R and 0.45R beneath the plane of the rotor. Upward velocities were obtained by downward pointed rakes positioned so that the total-pressure tubes were at the same elevations z/R as those of the upward pointing rakes. Total and static pressures were recorded for all tip Mach numbers above 0.45 and all pitch angles above 2° at the 0.75R station. Only a sampling of these results are presented in this report.

The sound-pressure level was measured at all test conditions above $M_t = 0.45$ and 0° pitch at the 0.75R station. These pressures were sensed by a microphone located 30 feet from the rotor center of rotation along a radial line inclined 5° below the plane of rotation. The indicated sound levels could be read to ±0.5 decibel; however, since the acoustical characteristics of the full-scale-tunnel test chamber are not known, these values may or may not be representative of the free-air sound.

RESULTS AND DISCUSSION

The results of the hovering investigation are given in three sections. The first part presents the hovering performance of the test rotor and compares it with the hovering performance of previously tested 10-foot-diameter rotors (ref. 1). The second section gives the rotor

drag-divergence characteristics and rate of growth of the profile-drag power. The last section offers a brief discussion on representative rotor downwash and sound measurements made during the tests.

Performance Characteristics

The rotor performance, extending through blade stall for a tip Mach number of 0.09, is presented in figure 6(a). At this tip Mach number, the Reynolds number along the blade varied from 62,000 at the 20-percent-radius station to 424,000 at the tip; it would therefore appear that the local Reynolds numbers at $M_t = 0.09$ were below the critical value. A maximum rotor mean lift coefficient of 0.88 was obtained at $M_t = 0.09$. This mean value compares favorably with the maximum section lift coefficient indicated at comparable Reynolds numbers by the data of reference 3. An adverse effect on section drag coefficient at this particular tip Mach number is indicated by the relatively higher values of rotor torque coefficient compared with data obtained for $M_t = 0.19$ to 0.38 which, in general, are in agreement with the data shown in figure 6(b) for $M_t = 0.45$.

Figure 6(b) gives the rotor performance over a range of tip Mach numbers from 0.45 to 0.98. Compressibility losses, evidenced by the departure of the curves from the curve for $M_t = 0.45$, are seen to follow the general trends of those in previous high-speed rotor investigations. (See refs. 1 and 4 to 8.) These compressibility losses become prominent at progressively lower thrust coefficients as the tip Mach number is increased. For a tip Mach number of 0.90 and above, the compressibility losses are present even at zero thrust coefficient.

The calculated performance at a tip Mach number of 0.45 is shown as a dashed curve in figure 6(b). This curve was calculated by means of a conventional strip analysis (ref. 9) in which lift-curve slope and drag coefficient were varied with Mach number along the blade span. The rotor tip loss was defined by the tip loss factor

$$B = 1 - \frac{\sqrt{2C_T}}{b}$$

The derivation of this equation is given in reference 1.

A comparison of the calculated and experimental performance curves at $M_t = 0.45$ indicates that, for a given thrust coefficient, the power required by the actual rotor is about 7 percent higher than that predicted by theory. This generally agrees with the results of reference 1.

Since the hub used in this investigation was smaller than that used in the investigation of reference 1, the discrepancy between the measured and calculated performance curves evidently does not result from rotor hub interference as was formerly suspected.

Inasmuch as the rotors of reference 1 and that of the present investigation have about the same solidity, it is of interest to compare the results by showing the variation of torque coefficient with tip Mach number for given values of thrust coefficient (fig. 7). From this figure two means of improving rotor static-thrust performance at high tip Mach number can be seen. One way is to reduce the thickness of the airfoil sections near the tip, and the other is to reduce, by judicious use of twist and taper, the portion of the lift carried by the outer high-speed part of the blades.

Rotor Drag-Divergence Characteristics

Drag divergence.- The point of inception and the rate of growth of compressibility losses are indicated in figures 8 and 9, which show the ratio of measured profile-drag torque coefficients to those measured at $M_t = 0.45$. The primary variable $\bar{c}_l$ in figure 8 is related to the overall performance of this particular rotor. Compressibility losses were first encountered at a tip Mach number of 0.63 and a rotor mean lift coefficient of 0.575. The primary variable $\alpha_{r,t}$ in figure 9 is related to the operating condition of those portions of the blade which are experiencing the greatest compressibility losses. It can be seen that, for similar combinations of $\bar{c}_l$ and M_t, the start and rate of growth of compressibility losses are comparable in magnitude with the results of previous investigations (refs. 1 and 4 to 8). At $M_t = 0.90$ and above, compressibility losses are present even at $\alpha_{r,t} = 0$.

The drag-divergence Mach number, defined as the Mach number at which the profile-drag-torque-coefficient ratio exceeds unity, may be determined as a function of $\alpha_{r,t}$ from figure 9. A comparison of the measured drag-divergence Mach number with that predicted by synthesized two-dimensional data from reference 4 is shown in figure 10. In general, the measured values follow trends predicted by the data of reference 4.

It may be noted that measured rotor drag-divergence Mach numbers for this particular rotor occur at higher Mach numbers than those predicted by two-dimensional data, whereas in reference 4 the reverse is true. One explanation of this difference is in the slightly different methods of determining the profile-drag-torque-coefficient ratios. Whereas the measured profile-drag-torque coefficients of this investigation were nondimensionalized by dividing by the measured value at

$M_t = 0.45$, the ratios of reference 4 were arrived at by dividing by the calculated $C_{Q,o}$ values.

Figure of merit.- The hovering efficiency of a rotor is often defined by the figure of merit. Variations of the figure of merit as a function of $\frac{C_T}{\sigma}$ and tip Mach number are given in figure 11. As the tip Mach number is increased, compressibility losses become more predominant. (See, also, figs. 8 and 9.)

These values of figure of merit have been compared with those of the fiber-glass rotor blade having an NACA 0012 airfoil section (ref. 1) at the same values of M_t and $\frac{C_T}{\sigma}$ and indicate that the all-metal rotor of the present investigation is more efficient at all test Mach numbers. The primary reason for the lower efficiency of the fiber-glass rotor is its smaller twist; additional factors reducing the efficiency are: slightly thicker airfoil sections (0012.3 as compared with 0011.75) and possible deformations of the fiber-glass rotor airfoil sections. Above $M_t = 0.86$ and $\frac{C_T}{\sigma} = 0.05$, the fiber-glass rotor blade having an NACA 64-series airfoil section (ref. 1) is more efficient than either of the rotor blades having NACA 0012 airfoil sections because of the thinner tip airfoil sections and greater taper and twist.

Thrust-horsepower ratio.- The relative efficiency of a rotor may also be shown dimensionally by the variation of the thrust per horsepower with disk loading and tip Mach number (fig. 12). For the test conditions covered, the maximum efficiency occurs at a disk loading of about 2 lb/sq ft and $M_t = 0.45$. As expected, an increase in tip Mach number decreases the efficiency of the rotor, and the disk loading at which maximum efficiency occurs is increased. Solid symbols in figure 12 indicate that the rotor is operating at or above drag divergence. Below $M_t = 0.77$, rotor drag divergence is not realized until a disk loading of the order of 11 to 14 lb/sq ft is reached. Above $M_t = 0.77$, the rotor drag divergence occurs at progressively lower disk loadings until at $M_t = 0.90$ compressibility effects are present at zero disk loading.

Additional Considerations of Operation at High Tip Mach Numbers

In addition to the force measurements discussed in the previous sections, measurements were made of the induced velocities beneath the

plane of the rotor and of the sound-pressure levels in the vicinity of the rotor. A brief discussion of the results of these measurements follows.

Rotor wake surveys.- The complete results of the wake surveys are not presented; however, the spanwise induced velocity distributions measured at rotor-blade tip Mach numbers of 0.45 and 0.82 are presented in figures 13(a) and 13(b), respectively. For convenience, the measured velocities have been nondimensionalized by dividing by the calculated average induced velocity v_o where

$$v_o = \Omega R\sqrt{\frac{C_T}{2}}$$

In general, the rotor wake appears to contract to about 0.82R at $z/R = -0.15$, and to 0.75R before reaching $z/R = -0.45$. This is in good agreement with the flow photographs of reference 10. It is also of interest to note that a superposition of the curves for the two tip Mach numbers ($M = 0.45$ and 0.82) would show little or no effect of Mach number on the spanwise induced velocity distribution.

The calculated induced velocities in the plane of the rotor are presented as dashed curves in figures 13(a) and 13(b). It can be seen that, as predicted by momentum theory, the average induced velocity well below the plane of the rotor is about twice that in the plane of the rotor.

Sound measurements.- Rotor operation at high tip Mach numbers is generally associated with a high noise level. An indication of the noise level associated with a rotor operating at high tip speeds may be seen in figure 14 which shows the variation of sound-pressure level with tip Mach number and rotor thrust coefficient.

It is evident from figure 14 that the major factor influencing the noise level is the tip speed. Smaller increases in noise are incurred by increases in thrust. The maximum noise level measured (141 db) occurred for the combination of the greatest thrust at the greatest tip speed.

CONCLUSIONS

An investigation of the hovering performance characteristics of an all-metal two-blade helicopter rotor 10 feet in diameter has been conducted in the Langley full-scale tunnel. The rotor blades tested had NACA 0012 airfoil sections, a 2/1 taper ratio, -12° of twist, and a

solidity of about 0.10. Tests were conducted over a range of tip Mach numbers from 0.09 to 0.98, and disk loadings to 22 pounds per square foot. Some measurements of induced velocities 15 percent and 45 percent of the radius beneath the plane of the rotor and of sound-pressure levels in the vicinity of the rotor were also made. As a result of these investigations, the following conclusions were reached:

1. Compressibility losses were first encountered at a tip Mach number of 0.63 and a rotor mean lift coefficient of 0.575. As the tip Mach number was increased, compressibility losses occurred at progressively lower values of rotor mean lift coefficient. At tip Mach numbers of 0.90 and above, compressibility losses were present even at zero rotor thrust.

2. Adverse effects of Reynolds number at very low tip speeds were only encountered at a tip Mach number of 0.09 (tip Reynolds number of 424,000).

3. At moderate tip speeds, torque requirements for a given thrust were about 7 percent larger than those predicted by theoretical calculations of the rotor hovering performance.

4. A comparison of the present rotor with those tested in the investigation reported in NACA Research Memorandum L58B19 indicates that above a tip Mach number of 0.86 hovering efficiency is improved by a reduction in tip airfoil thickness and by increased twist and taper.

5. The induced velocity distribution beneath the plane of the rotor is largely unaffected by tip Mach number within the range of these tests.

6. The noise associated with a rotating rotor is primarily a function of tip speed and secondarily a function of thrust.

Langley Research Center,
National Aeronautics and Space Administration,
Langley Field, Va., December 23, 1959.

REFERENCES

1. Jewel,Joseph W., Jr., and Harrington, Robert D.: Effect of Compressibility on the Hovering Performance of Two 10-Foot-Diameter Helicopter Rotors Tested in the Langley Full-Scale Tunnel. NACA RM L58B19, 1958.

2. DeFrance, Smith J.: The N.A.C.A. Full-Scale Wind Tunnel. NACA Rep. 459, 1933.

3. Jacobs, Eastman N., and Sherman, Albert: Airfoil Section Characteristics as Affected by Variations of the Reynolds Number. NACA Rep. 586, 1937.

4. Carpenter, Paul J.: Lift and Profile-Drag Characteristics of an NACA 0012 Airfoil Section as Derived From Measured Helicopter-Rotor Hovering Performance. NACA TN 4357, 1958.

5. Powell, Robert D., Jr.: Compressibility Effects on a Hovering Helicopter Rotor Having an NACA 0018 Root Airfoil Tapering to an NACA 0012 Tip Airfoil. NACA RM L57F26, 1957.

6. Shivers, James P., and Carpenter, Paul J.: Experimental Investigation on the Langley Helicopter Test Tower of Compressibility Effects on a Rotor Having NACA 63_2-015 Airfoil Sections. NACA TN 3850, 1956.

7. Shivers, James P., and Carpenter, Paul J.: Effects of Compressibility on Rotor Hovering Performance and Synthesized Blade-Section Characteristics Derived From Measured Rotor Performance of Blades Having NACA 0015 Airfoil Tip Sections. NACA TN 4356, 1958.

8. Powell, Robert D., Jr., and Carpenter, Paul J.: Low Tip Mach Number Stall Characteristics and High Tip Mach Number Compressibility Effects on a Helicopter Rotor Having an NACA 0009 Tip Airfoil Section. NACA TN 4355, 1958.

9. Gessow, Alfred, and Myers, Garry C., Jr.: Aerodynamics of the Helicopter. The MacMillan Co., c.1952, pp. 72-73.

10. Taylor, Marion K.: A Balsa-Dust Technique for Air-Flow Visualization and Its Application to Flow Through Model Helicopter Rotors in Static Thrust. NACA TN 2220, 1950.

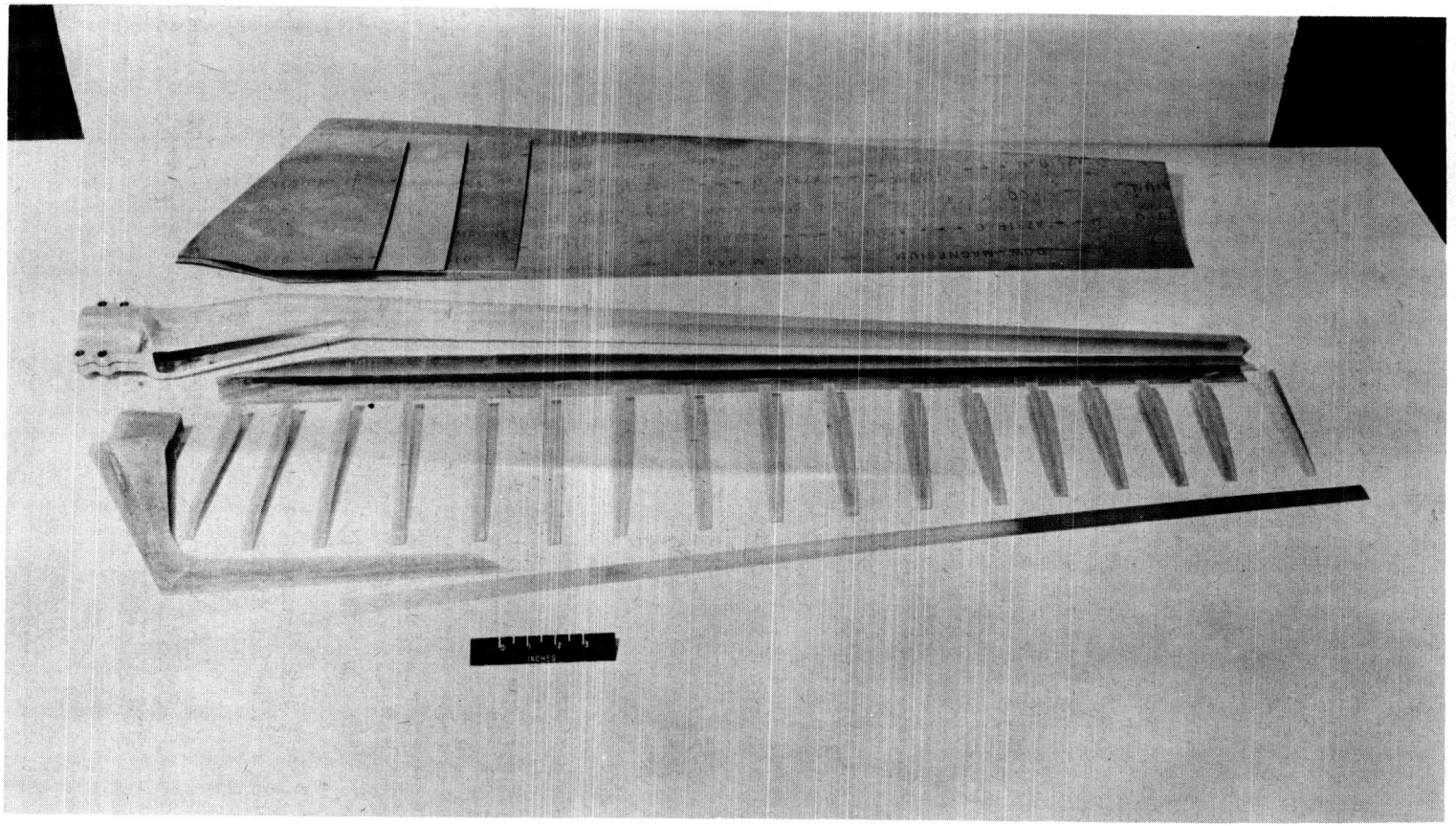

Figure 1.- Components of rotor blade before final assembly. L-58-549a

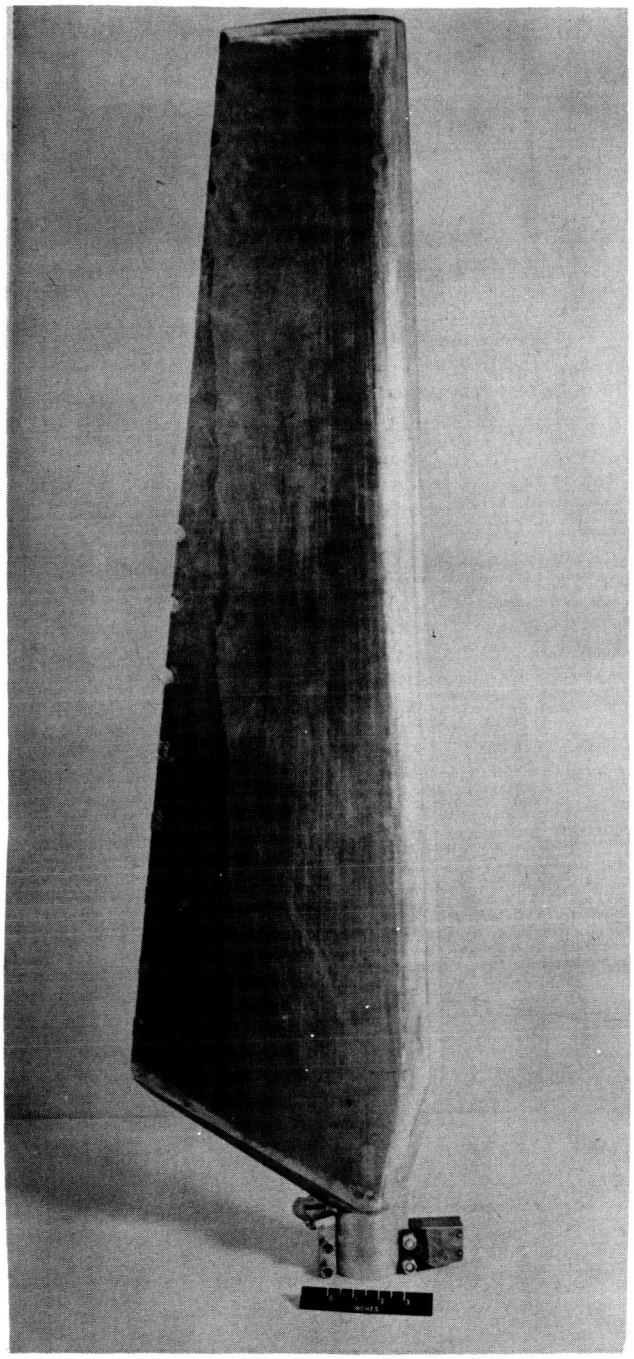

L-58-867a

Figure 2.- All-metal helicopter rotor blade having NACA 0012 airfoil sections used in hovering tests.

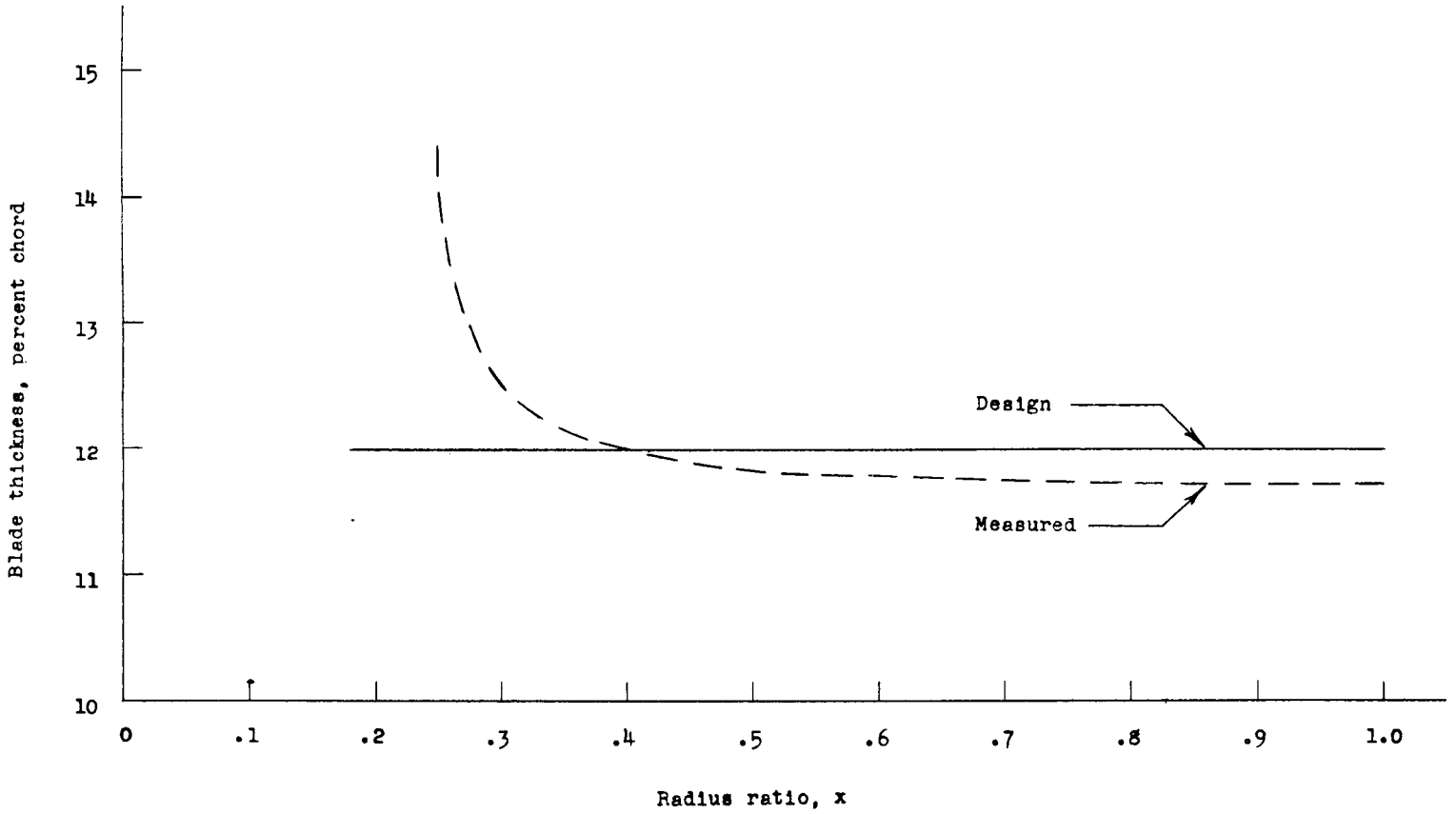

Figure 3.- Spanwise thickness distribution of all-metal helicopter rotor blade having NACA 0012 airfoil section.

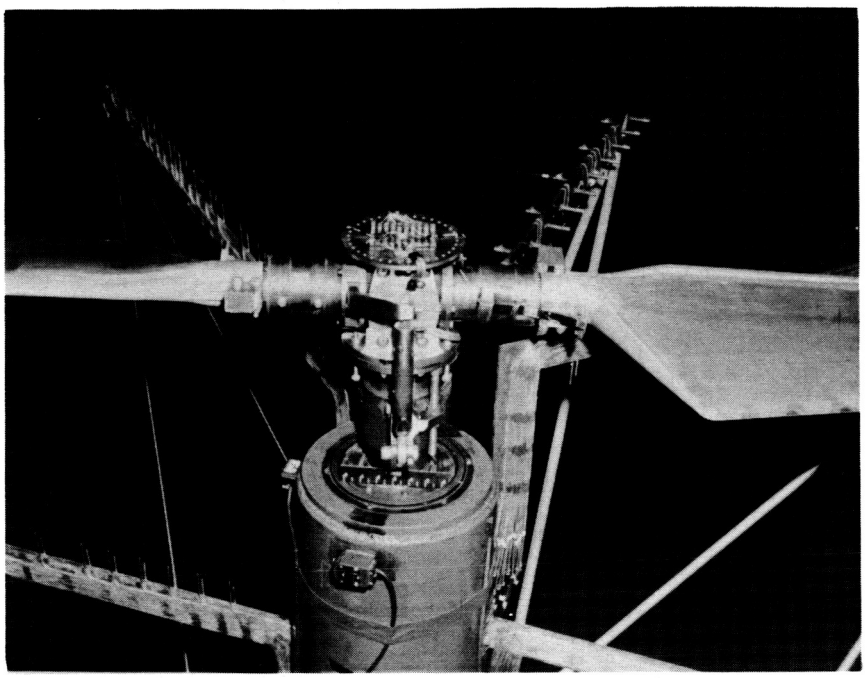

Figure 4.- General view of rotor head. L-58-1138a

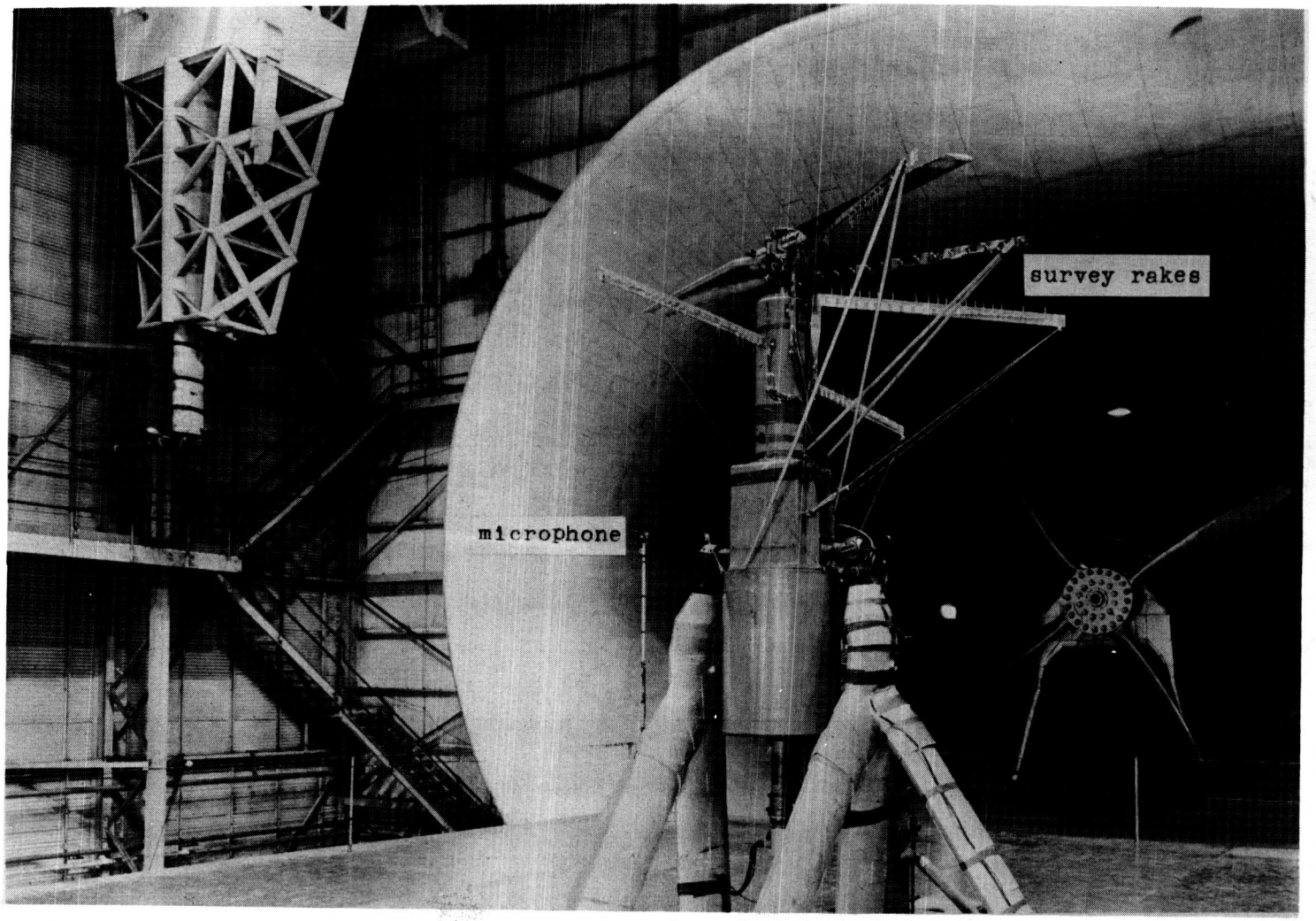

L-58-1132a.1

Figure 5.- Rotor test setup mounted in Langley full-scale-tunnel test section.

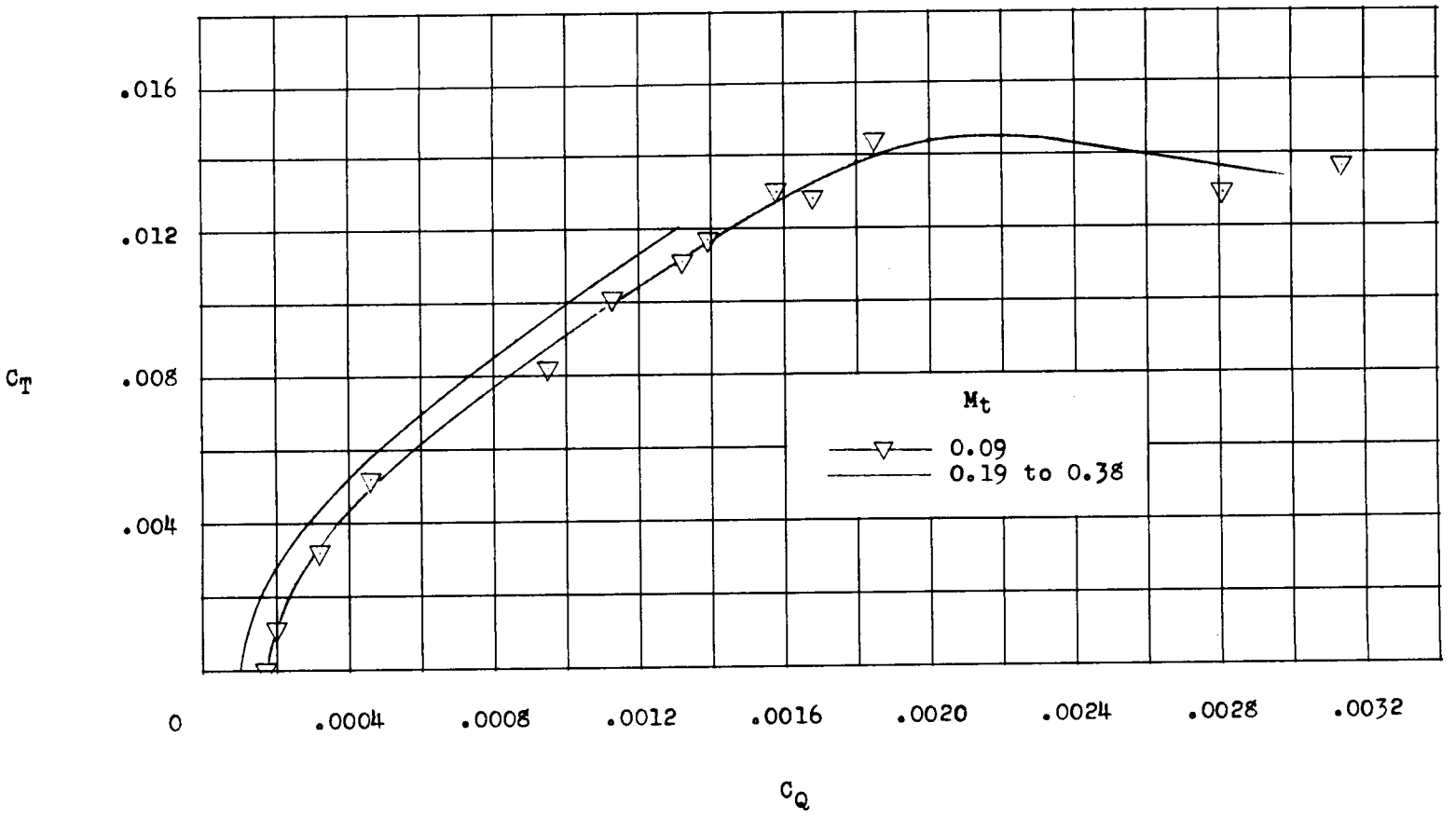

(a) M_t = 0.09 to 0.38; $N_{Re,t}$ = 424,000 to 1,702,000.

Figure 6.- Hovering performance of an all-metal 10-foot-diameter rotor having NACA 0012 airfoil section, a 2/1 taper ratio, and -12° of twist over a range of tip Mach numbers from 0.09 to 0.98. σ = 0.099.

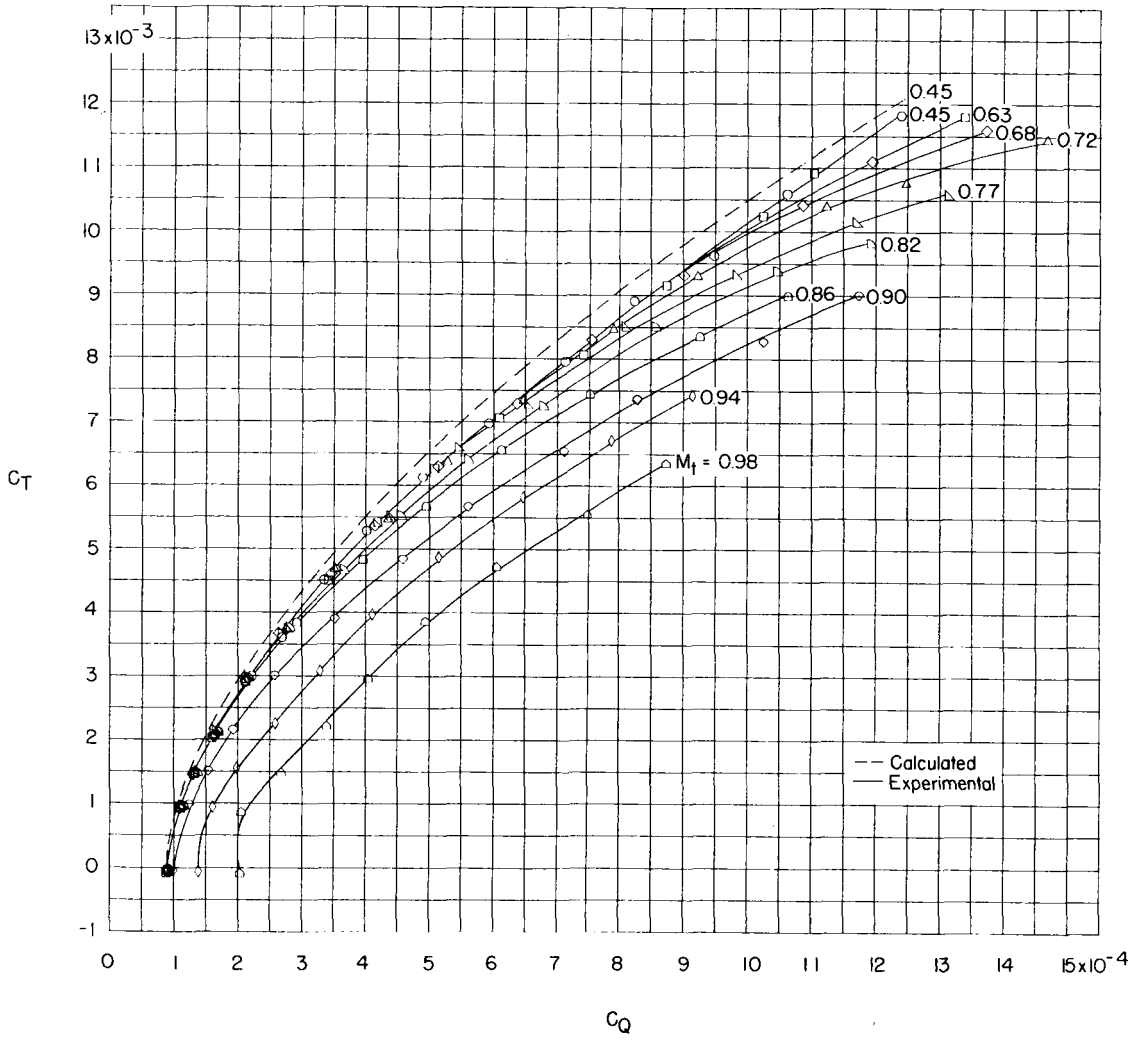

(b) M_t = 0.45 to 0.98. (C_l and $C_{d,o}$ varied with Mach number along the blade for calculated curve.)

Figure 6.- Concluded.

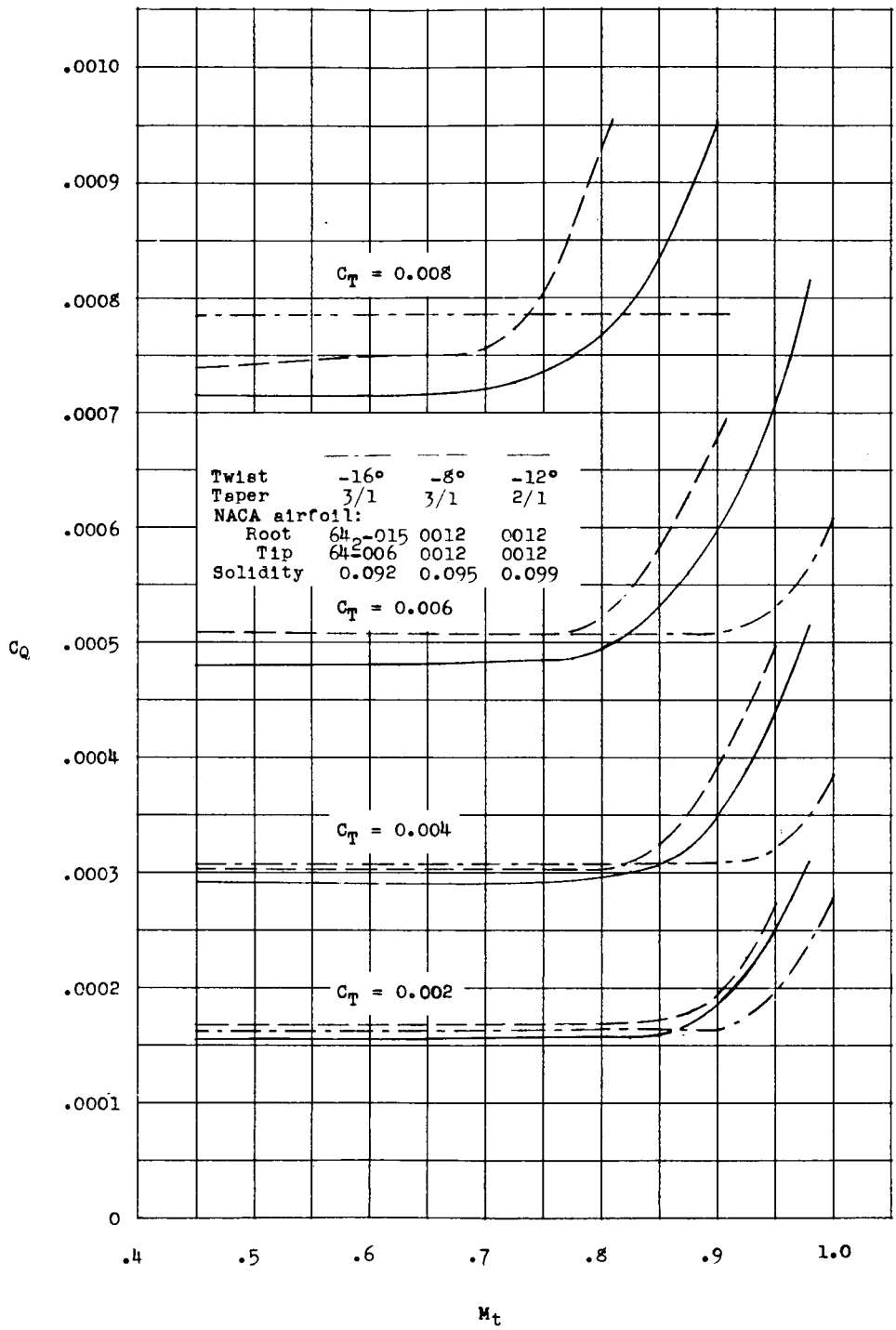

Figure 7.- Comparison of the hovering performance of three 10-foot-diameter rotors tested in the Langley full-scale tunnel.

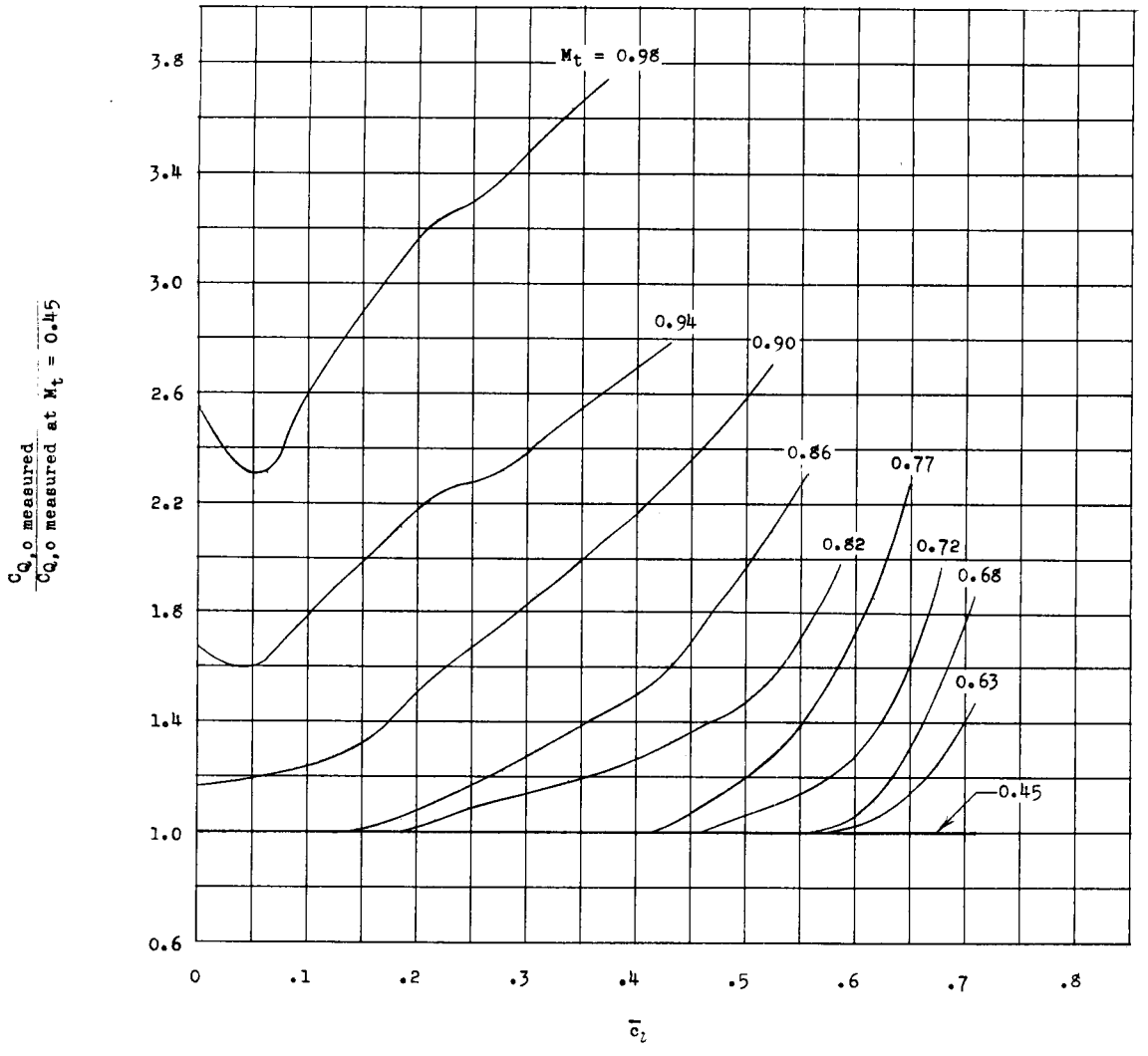

Figure 8.- Effect of mean lift coefficient and tip Mach number on profile-drag-torque-coefficient ratio of rotor blade.

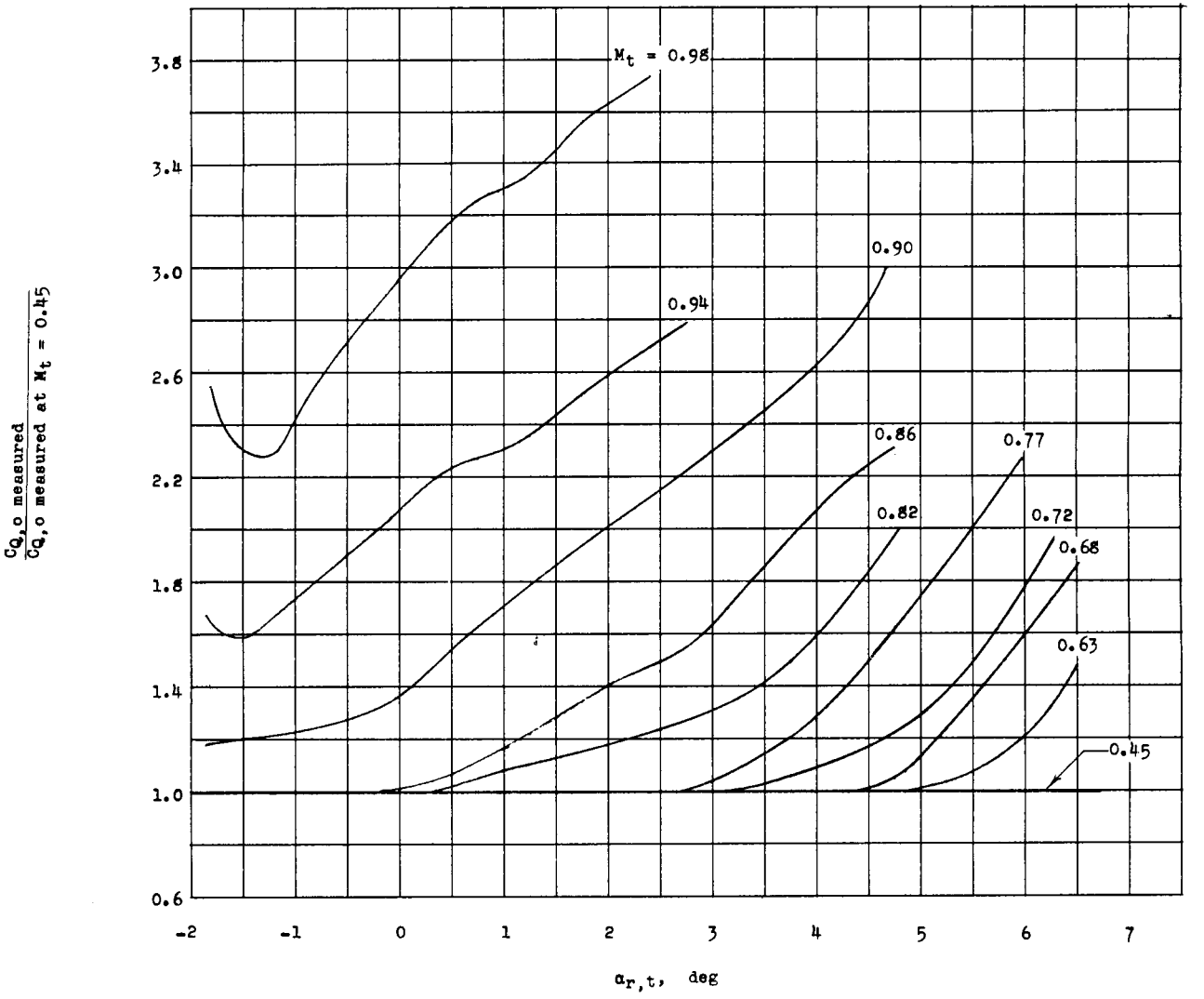

Figure 9.- Effect of tip angle of attack and tip Mach number on profile-drag-torque-coefficient ratio of rotor blade.

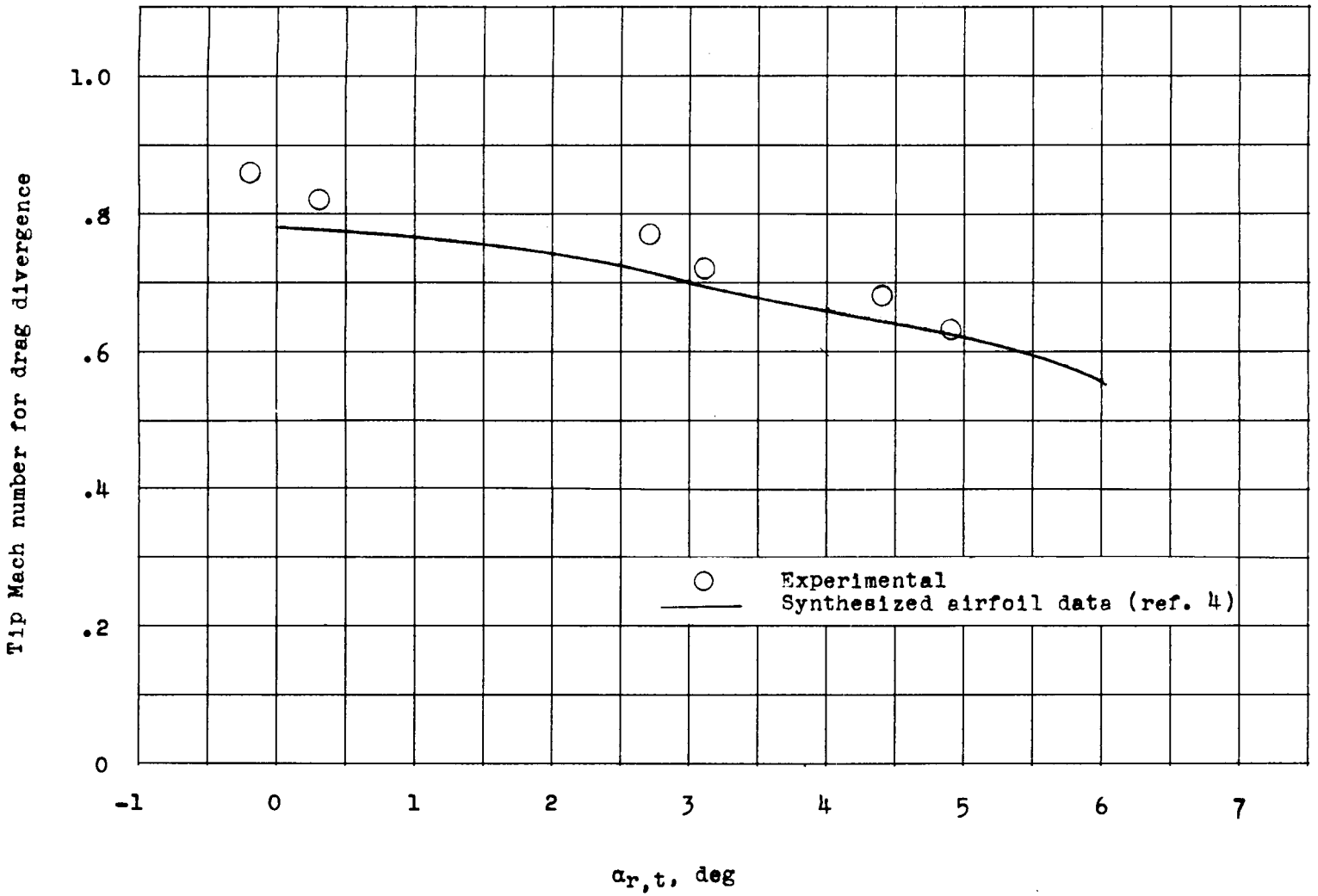

Figure 10.- Comparison of measured drag-divergence Mach number with the drag-divergence Mach number predicted by synthesized two-dimensional data.

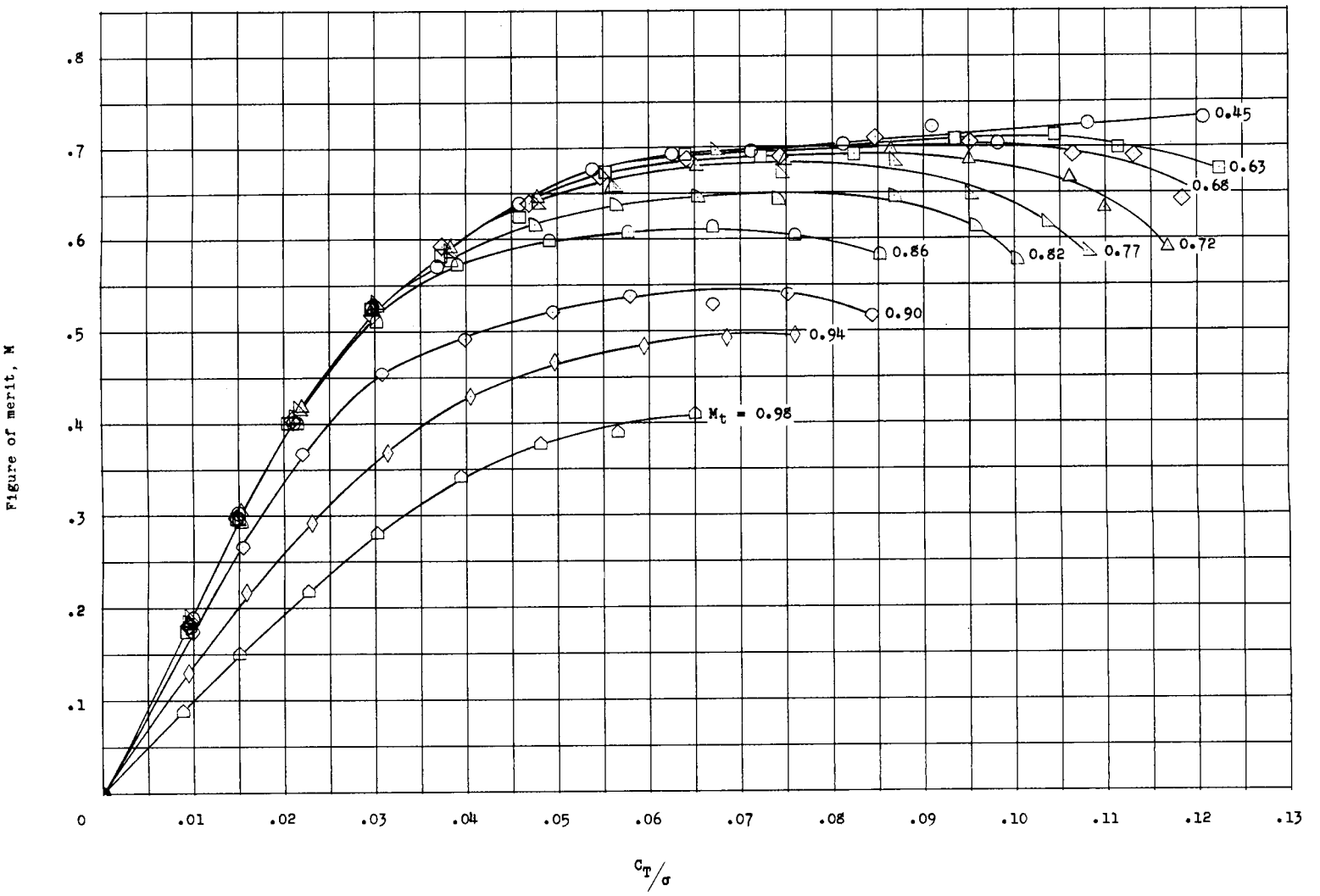

Figure 11.- Effect of tip Mach number on figure of merit of an all-metal 10-foot-diameter rotor having NACA 0012 airfoil section, a 2/1 taper ratio, and -12° of twist. σ = 0.099.

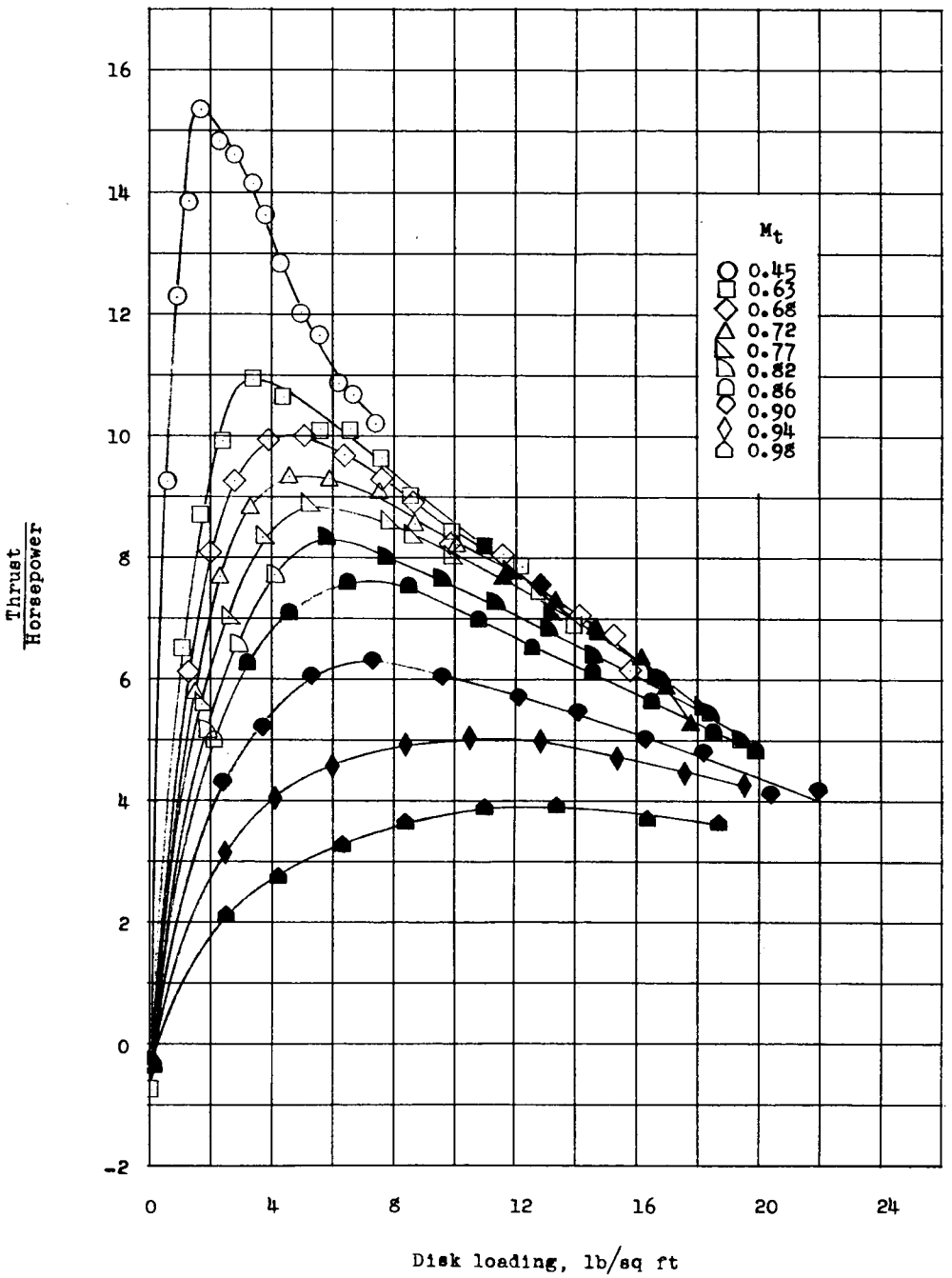

Figure 12.- Effect of disk loading and Mach number on the power loading of an all-metal 10-foot-diameter rotor having NACA 0012 airfoil section, a 2/1 taper ratio, and -12° of twist. $\sigma = 0.099$. (Solid symbols indicate operation of the rotor at or above drag-divergence.)

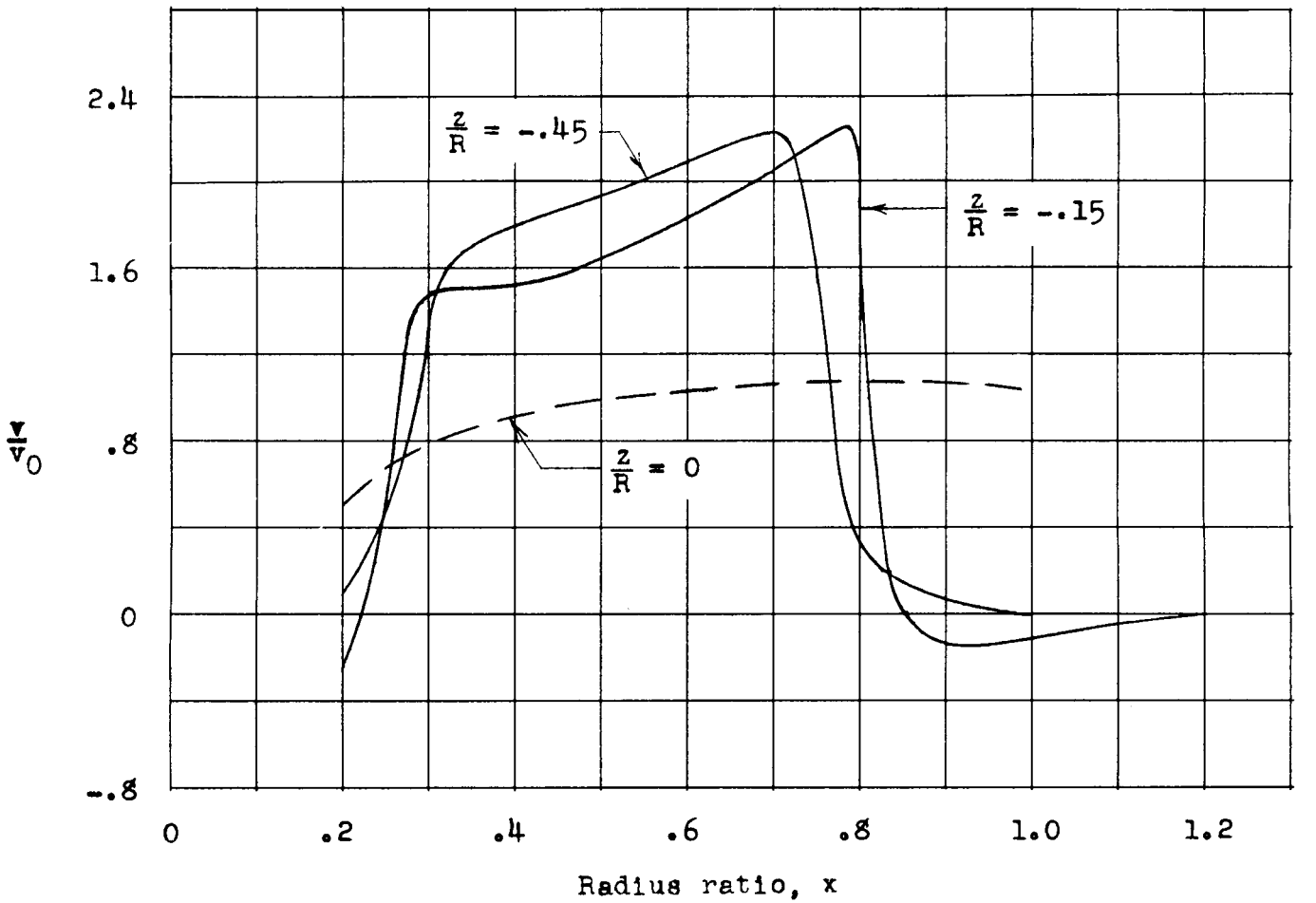

(a) $M_t = 0.45$; $\theta_t = 11^\circ$.

Figure 13.- Measured and theoretical induced velocity distributions across the wake of an all-metal 10-foot-diameter rotor having NACA 0012 airfoil section, a 2/1 taper ratio, and -12° of twist. $\sigma = 0.099$.

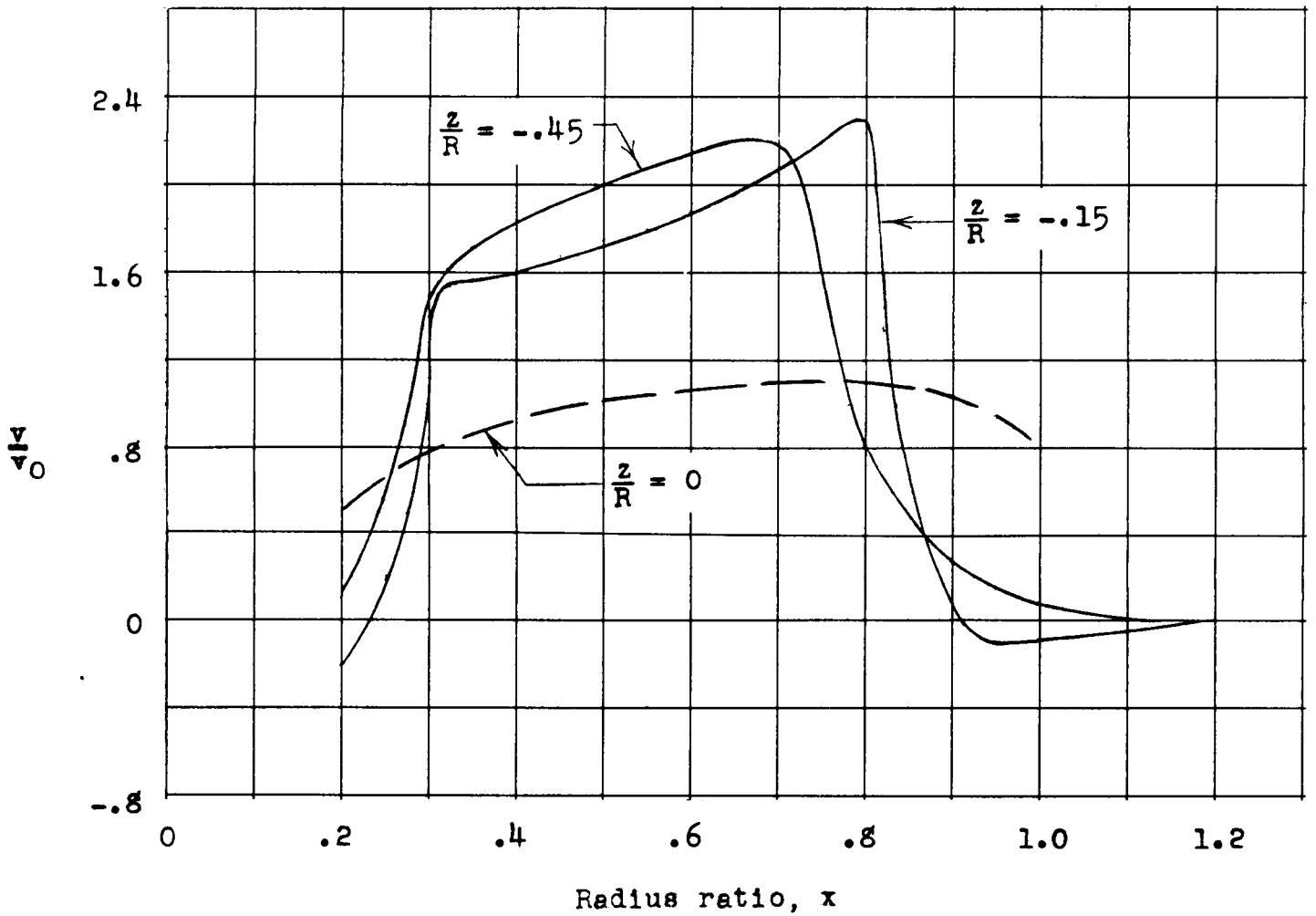

(b) $M_t = 0.82$; $\theta_t = 9^o$.

Figure 13.- Concluded.

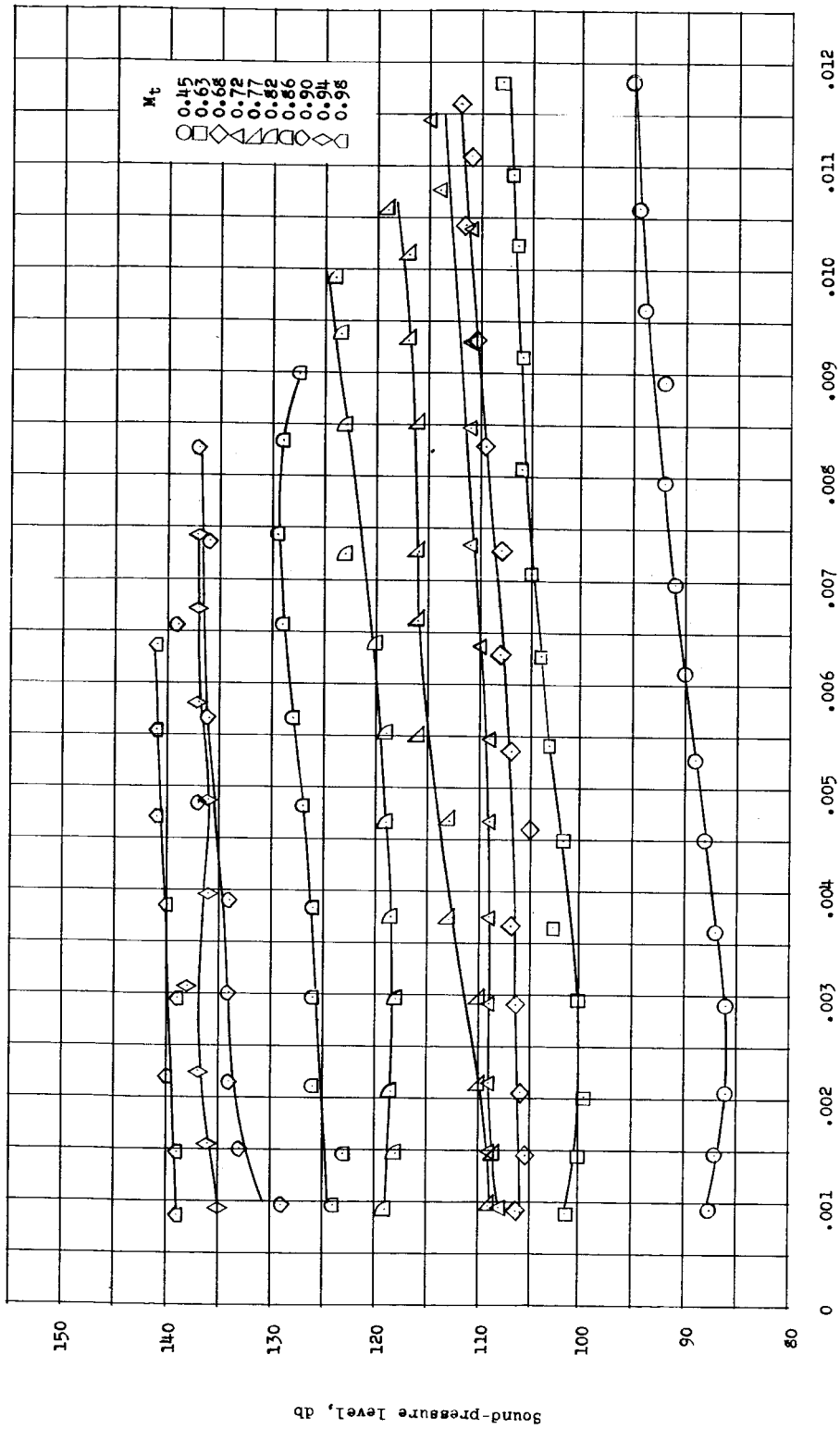

Figure 14.- Variation of sound-pressure level with tip Mach number and thrust coefficient. Sound-pressure level measured 30 feet from center of rotor along a radial line inclined 5° below the plane of the rotor.

L-700